International Journal of Adhesion & Adhesives 96 (2020) 102464

Contents lists available at ScienceDirect

International Journal of Adhesion and Adhesives

journal homepage: http://www.elsevier.com/locate/ijadhadh

Adhesion of a water droplet on inclined hydrophilic surface and internal fluidity

Abdullah Al-Sharafi [a,b], Bekir S. Yilbas [a,c,*], Haider Ali [a], H. Al-Qahtani [a]

[a] Mechanical Engineering Department, KFUPM, Dhahran, 31261, Saudi Arabia
[b] Researcher at K.A.CARE Energy Research & Innovation Center at Dhahran, Saudi Arabia
[c] Senior Researcher at K.A.CARE Energy Research & Innovation Center at Dhahran, Saudi Arabia

ARTICLE INFO

Keywords:
Water droplet
Inclined hydrophilic surface
Adhesion
Flow filed

ABSTRACT

A water droplet attachment on a hydrophilic surface with inclination is investigated. The influence of droplet size and the inclination angle of the surface on the droplet adhesion are examined. Height and lateral extension of the droplet on the inclined hydrophilic surface are formulated and the findings are compared with the experimental data. The hydrodynamic response of the droplet due to inclination of the surface is simulated and the flow field inside the droplet is predicted for various droplet inclination angles of the surface and the droplet size. An experiment is designed to validate the flow field predicted inside the droplet via incorporating particle image velocimetry (PIV). It is found that the velocity predicted agrees well with the PIV data. A circulation cell is developed inside the droplet and the rotational center and the strength of the fluid circulation change with the inclination angle and the droplet size. The adhesion force increases with increasing inclination angle of the surface and the droplet size. The shear force generated at the wetted surface contributes to the adhesion force; however, this contribution is not significant.

1. Introduction

The self-cleaning of surfaces becomes critical towards minimizing efforts required for surface cleaning processes. Climate change gives rise to regular dust storms around the Globe, particularly in the Middle East, while soiling of the surfaces of energy harvesting devices such as photovoltaic panels and concentrated solar reflectors. In general, water droplets are possible candidates for removing dust particles from surfaces [1]. The use of water droplets minimizes excessive clean water usage in surface-cleaning applications. Although hydrophobic surface characteristics are favorable for rolling water droplets on surfaces so as to generate self-cleaning affects, the presence of local textural asperities can give rise to high hysteresis of the droplet contact angles while ceasing the rolling off of droplets on surfaces. On the other hand, water droplets on hydrophilic surfaces can resemble similar behavior as those on hydrophobic surfaces with high contact angle hysteresis. In this case, the adhesion force generated at the surface, due to surface tension force, gives rise to pinning of the droplets thus preventing the droplets from sliding on the surface. When the surface is inclined, droplet bulging results from the applied gravitational force and the droplet motion is defined through the force balance including adhesion, gravity, and shear forces. Increasing droplet size enhances both gravitational and adhesion forces. The enhancement of adhesion force is associated with the increased circumference of the wetted surface for large droplet volumes. Shear force is related to the shear stress at the wetted surface because of the internal fluidity of the droplet. In this case, the rate of fluid strain in the vicinity of the wetted surface plays an important role for the enhancement of shear force. The hydrodynamic behavior of the droplet fluid alters the rate of the fluid strain during the surface inclination because of the droplet bulging during the inclination. The change of the droplet shape via bulging modifies the location of the droplet centroid and center of mass, which in turn modifies the force balance on the inclined surface. Consequently, investigation of droplet deformation and the force balance on the inclined hydrophilic surface becomes essential.

Considerable research studies have been carried out to examine the behavior of water droplets on surfaces. Droplet adhesion on hydrophobic and hydrophilic surfaces have been of interest in terms of thermal processes, such as heating, condensation, and evaporation. The droplet adhesion was mainly governed by the surface texture parameters and surface energy [2–4]. In the case of surface texture, the size of the microstructure pitch and density of the nanostructures were important for droplet adhesion on surfaces, which possessed rose petal textures

* Corresponding author. Mechanical Engineering Department, KFUPM, Dhahran, 31261, Saudi Arabia.
E-mail address: bsyilbas@kfupm.edu.sa (B.S. Yilbas).

https://doi.org/10.1016/j.ijadhadh.2019.102464

Available online 28 October 2019

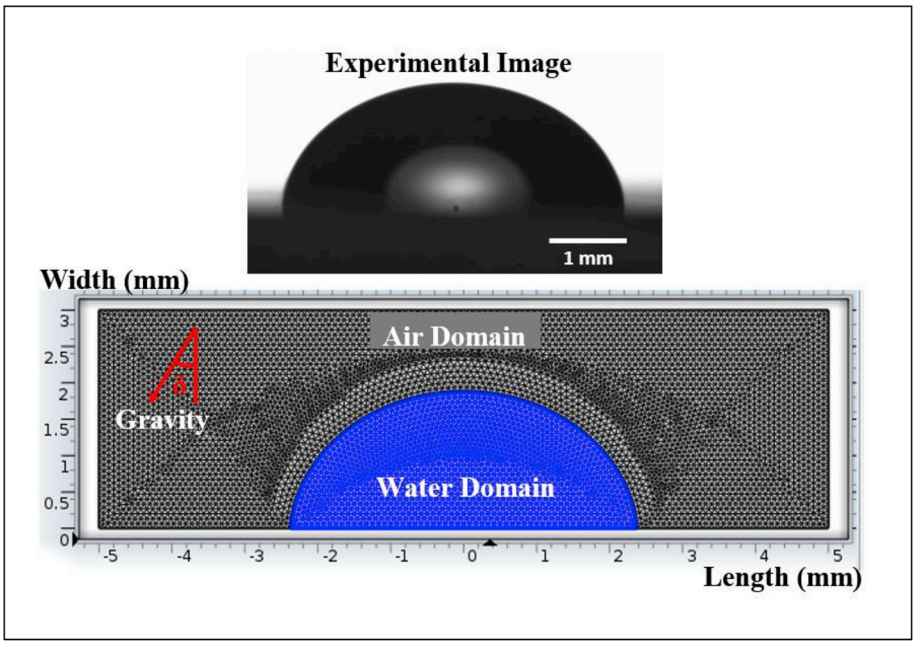

Fig. 1. Actual droplet image on the hydrophilic surface and Mesh used in the simulations.

[2]. In addition, micro size dots and conical posts on surfaces have been shown to create texture effects on droplet adhesion [5,6]. Heat transfer from textured surfaces has been shown to lower surface temperature while lowering pressure in the air gaps at an interface. This, in turn, influenced droplet adhesion at the surface while altering the wetting state of the surface [7]. The reversible switching of surface wettability remained critical for the droplet dynamics and its adhesion on the surface [8]. Switching the wetting state from hydrophobic to hydrophilic has been shown to reduce droplet adhesion and enhance droplet sliding on a surface [8]. The force balance on a droplet was critical for the droplet motion on hydrophobic surfaces [9,10]; in which case, reducing droplet contact angle could cause the breaking up of droplets into certain patterns on a surface [10]. On the other hand, liquid droplet adhesion on surfaces finds application in various engineering and medical fields [11–14]. For example, droplet adhesion could be utilized as a promising technology for recycling of emulsions in microfluidic devices [11], bio-detection via surface reactions [12], and cell spreading on surfaces [13]. In general, surface texturing towards achieving nanostructures has been shown to be important in the design of micro-electronic systems and functional devices for biomedical applications [14].

Although droplet adhesion on hydrophobic and hydrophilic surfaces has been studied previously [15,16], the main focus was investigating the heat transfer characteristics of a sessile droplet on horizontal surfaces with the important effects of inclination angle and droplet size on the adhesion of a droplet on hydrophilic surfaces left for a future study. In addition, when a sessile droplet on a hydrophobic surface is inclined, the force balance changes while modifying the droplet shape on the surface. In this case, the hydrodynamic response of a droplet liquid can generate a shear layer in the interfacial region between the droplet and the surface. This, in turn, gives rise to generation of a shear force contributing to the overall force balance on the droplet. Consequently, in the present study, droplet adhesion on a hydrophilic surface is considered and the flow field inside the droplet is simulated for various inclination angles of the hydrophilic surface. The adhesion force variation and the droplet shape characteristics are evaluated for different droplet sizes and various inclination angles of the surface. Water is used as the working fluid inside the droplet.

2. Modelling and experimental study of droplet internal fluidity

The internal fluidity of a droplet on an inclined hydrophilic surface is simulated in line with the experimental conditions. The actual geometric features of a droplet prior to inclination and the typical meshes used in the simulations are shown in Fig. 1. COMSOL Multiphysics software [17] is incorporated to simulate the flow field inside the droplet. Laminar two-phase flow, moving mesh interface is used for the simulations while incorporating the Arbitrary Lagrangian–Eulerian (ALE) formulation in the computations [18]. Since temperature is kept constant during the experiments, an isothermal flow is assumed in the simulations. The arrangements of the numerical details of the droplet fluidity are given in Appendix 1.

A glass wafer was used to simulate the hydrophilic surface. A goniometer Kyowa (model - DM 501) was used to conduct sessile drop tests for the measurement of droplet contact angle, which was varied within 73° – 82°. The contact angle measurements were repeated 12 times at different locations on the surface. The experimental error estimated was in the order of 5%, i.e. the ranges of water droplet contact angle and the error estimated are 73°±3.5° - 82°±4°.

A test rig was designed and constructed to test the dynamic behavior of the droplets on the inclined hydrophilic surface. In this case, a high speed camera (Dantec) was used to record the bulging of the droplet of 25 μL located on the hydrophilic surface with different inclination angles. Fig. 2 shows images of a droplet of $V_d = 25$ μL on the inclined hydrophilic surface with the range of the inclination angle of $\delta = 20°$ to 80°. The velocity contours, which are obtained from the simulations incorporating the identical boundary conditions of the experiments, are also shown in Fig. 2.

In order to validate the model studied, particle image velocimetry (Dantec PIV) was used to monitor particle velocities inside the droplet. In this case, a sessile droplet of $V_d = 60$ μL volume was used to simulate the flow field numerically and monitor the flow velocities using PIV. Hollow glass particles of 10 μm size were used in the droplet liquid to monitor and trace the particle velocities inside the droplet during the inclination. The governing equation of momentum was solved after incorporating the hollow glass particles in the solution domain via using the discrete phase model. Since the hollow glass particle concentration is low (3%) in the carrier fluid (water), effective properties were incorporated in the governing equations. The incompressible flow field was

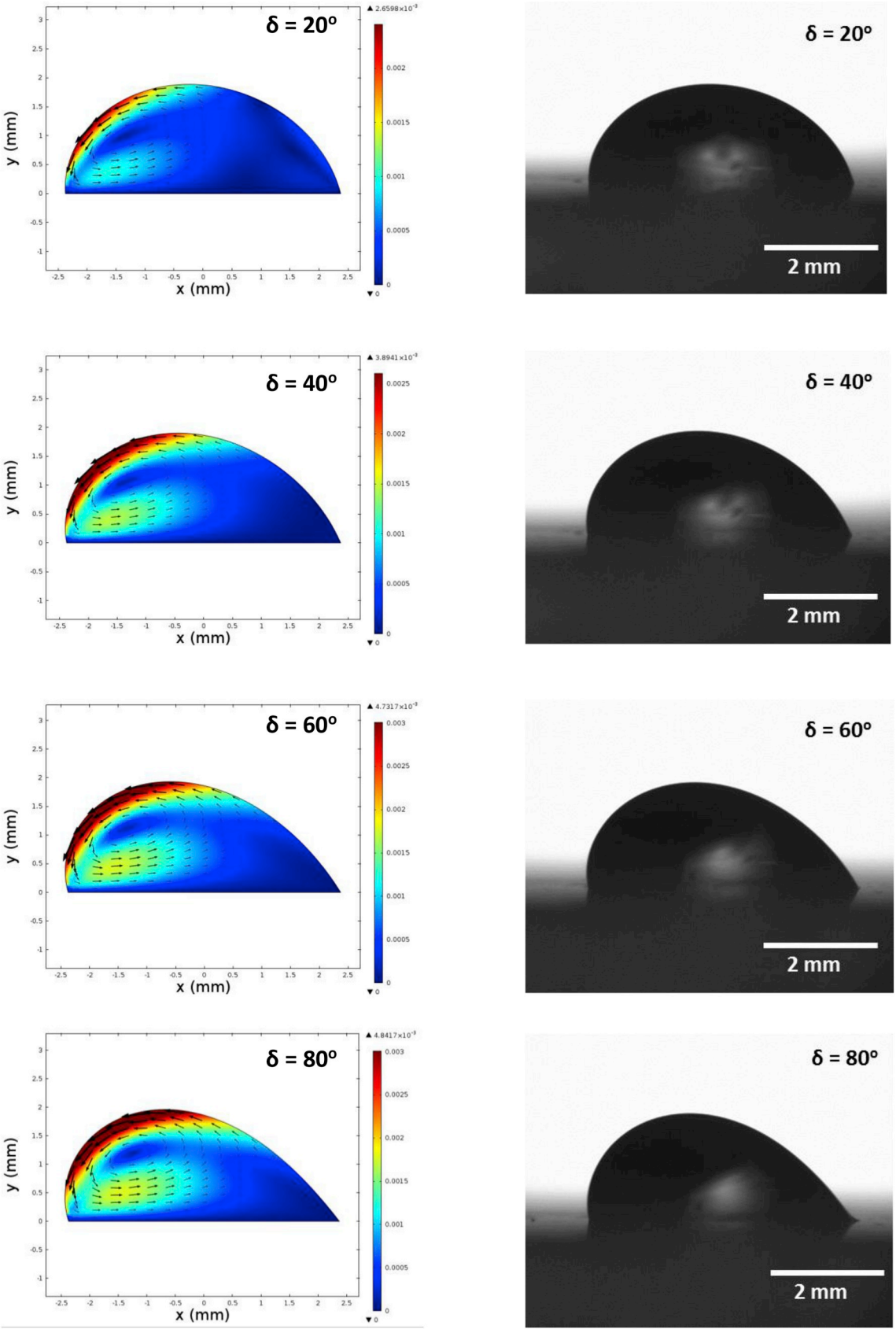

Fig. 2. Velocity contours obtained from the simulation inside the droplet and actual droplet images at different inclination angles for 25 μL droplet.

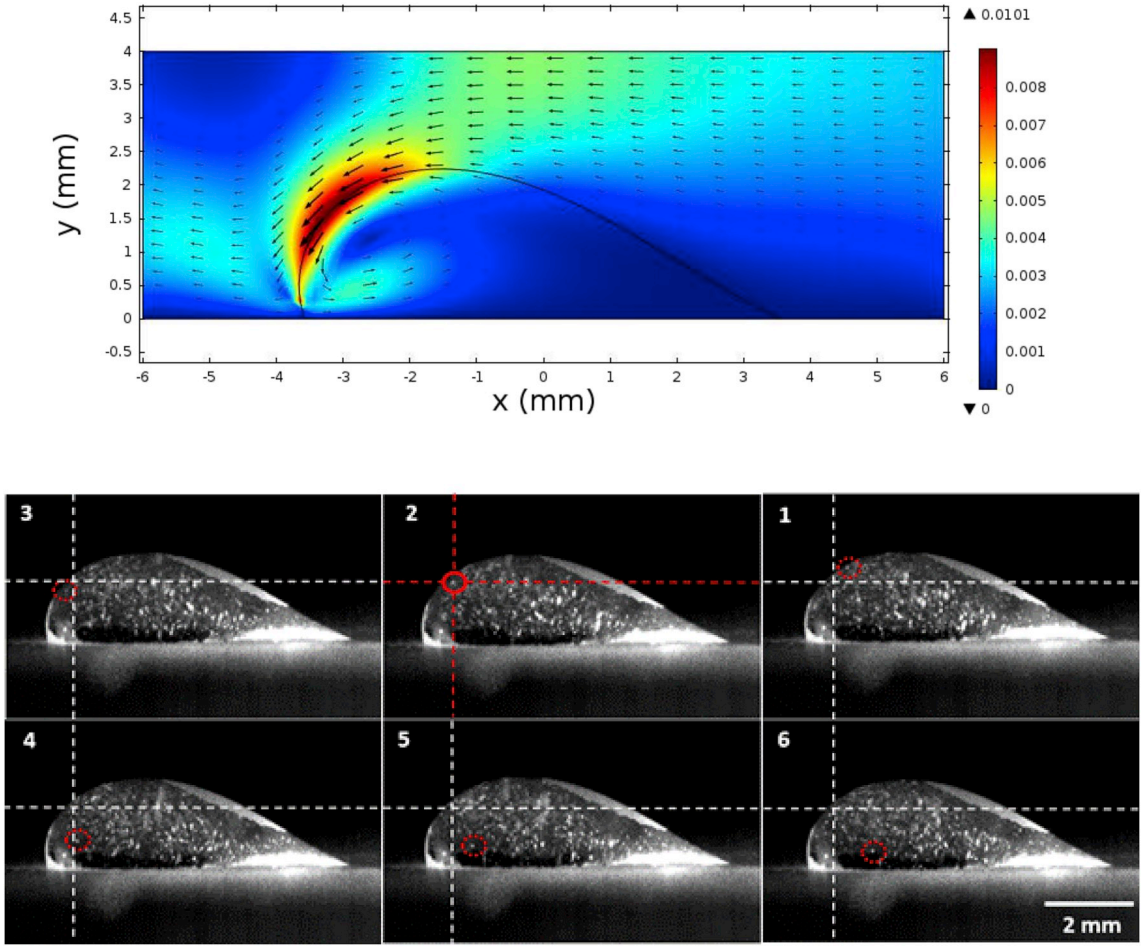

Fig. 3. Simulation results of velocity contours after 45 s and PIV images of particles inside the droplet for various durations. The time difference between each frame for PIV images is 3.26 s. The droplet size is 60 μL and inclination angle of the surface is $\delta = 45^{\circ}$.

Table 1
Simulation results and experimental data for velocity of particles.

Particle #	X (mm)	Y (mm)	Experiment V (m/s)	Simulation V (m/s)
1	0.1500	1.6627	0.0009	0.0010
2	−0.4359	1.9290	0.0017	0.0018
3	−0.9152	2.0711	0.0027	0.0025
4	−1.6610	2.1598	0.0048	0.0050
5	−2.1581	2.1066	0.0064	0.0065
6	−2.5309	2.0178	0.0080	0.0082
7	−2.8860	1.8403	0.0092	0.0097
8	−3.0814	1.6449	0.0090	0.0095
9	−3.2589	1.4319	0.0087	0.0083
10	−3.4720	1.0945	0.0081	0.0080
11	−3.5430	0.7039	0.0057	0.0055
12	−3.4720	0.4909	0.0036	0.0039
13	−3.2234	0.2601	0.0034	0.0030
14	−2.8150	0.2068	0.0029	0.0030

considered and the field equations were solved numerically in line with the experimental conditions. The formulation of the governing equations and numerical analysis are not given herein, but the details can be found in the previous study [19]. The images of the particles and their positions inside the droplet as obtained from PIV, are shown in Fig. 3. In addition, the flow velocities measured from PIV and predicted from the multi-physics code are given in Table 1. It is evident that the particle velocities predicted from the multi-physics code and obtained from the experiment are in good agreement. However, some small discrepancies between both results are related to computational errors, such as round off errors, and the experimental error based on the measurement repeatability which is in the order of 6%.

3. Results and discussion

The droplet sliding and rolling at the surface are associated with the net adhesion force resulted at the surface. Although inclination of the hydrophilic surface increases the lateral component of the gravitational force for droplet slipping and/or rolling at the surface, droplet contact angle hysteresis is critically important for the dynamic movement of the droplet at the surface. Unlike the hydrophobic surfaces, contact angle hysteresis and the wetted area of the droplet remain large for the hydrophilic surfaces. In addition, fluid acceleration due to the flow current generated in the droplet during the inclination of the surface contributes to both deformation of the droplet shape and the adhesion force between the droplet and the inclined surface. The rolling and/or sliding of the droplet is not observed during the experiments for the droplet volumes considered ($5\ \mu L \leq \forall \leq 25\ \mu L$) in the present study. The advancing and receding angles of the droplet with different sizes and the inclination angles of the solid surface are given in Table 2. The droplet contact angle hysteresis (θ_R - θ_A) increases with inclination angle and droplet size, which in turn alters the values of the lateral adhesion force and the extent of droplet bulging. The lateral adhesion force can be formulated heuristically by approximating the three-phase contact line with a single ellipse [20]. In addition, the experimentally obtained polynomial function can be incorporated for the dependence of the contact angle on the position along the three-phase contact line when formulating the lateral adhesion force [21]. The adhesion force can be written as:

Table 2
Advancing (θ_A), receding (θ_R) and hysteresis (θ_R - θ_A) of the water droplets on inclined hydrophilic surface for various droplet sizes and inclination angles.

$V_d = 5$ μL				$V_d = 10$ μL			
δ (deg)	θ_a (deg)	θ_R (deg)	(θ_a - θ_R) (deg)	δ (deg)	θ_a (deg)	θ_R (deg)	(θ_a - θ_R) (deg)
10	80.79	80.15	0.64	10	88.48	78.72	9.76
20	87.34	78.61	8.73	20	89.67	76.98	12.69
30	88.14	77.6	10.54	30	90.71	74.48	16.23
40	90	76.35	13.65	40	91.79	72.5	19.29
50	91.31	75.43	15.88	50	92.9	69.69	23.21
60	92.62	72.65	19.97	60	94.37	68.7	25.67
70	92.78	70.38	22.4	70	95.67	66.8	28.87
80	93.47	69.16	24.31	80	96.82	64.45	32.37
90	94.6	68.55	26.05	90	97.62	62.25	35.37
Vd = 15 μL				Vd = 20 μL			
δ (deg)	θ_a (deg)	θ_R (deg)	(θ_a - θ_R) (deg)	δ (deg)	θ_a (deg)	θ_R (deg)	(θ_a - θ_R) (deg)
10	82.21	78.88	3.33	10	88.85	82.93	5.92
20	84.35	75.7	8.65	20	90.2	79.91	10.29
30	87.18	73.39	13.79	30	92	77.3	14.7
40	89.19	70.2	18.99	40	93.5	74.6	18.9
50	91.88	67.83	24.05	50	95.45	71.6	23.85
60	93.62	65.18	28.44	60	97	68.4	28.6
70	95.89	61.59	34.3	70	98.7	65.6	33.1
80	98.62	59.83	38.79	80	100.2	63	37.2
90	100.62	56.63	43.99	90	101.73	59.97	41.76

$V_d = 25$ μL			
δ (deg)	θ_a (deg)	θ_R (deg)	(θ_a - θ_R) (deg)
10	88.85	77.42	11.43
20	90.81	73.7	17.11
30	93	70.3	22.7
40	94.62	66.71	27.91
50	96.6	63	33.6
60	98.5	60	38.5
70	100.5	56	44.5
80	102.4	52.5	49.9
90	104.27	48.92	55.35

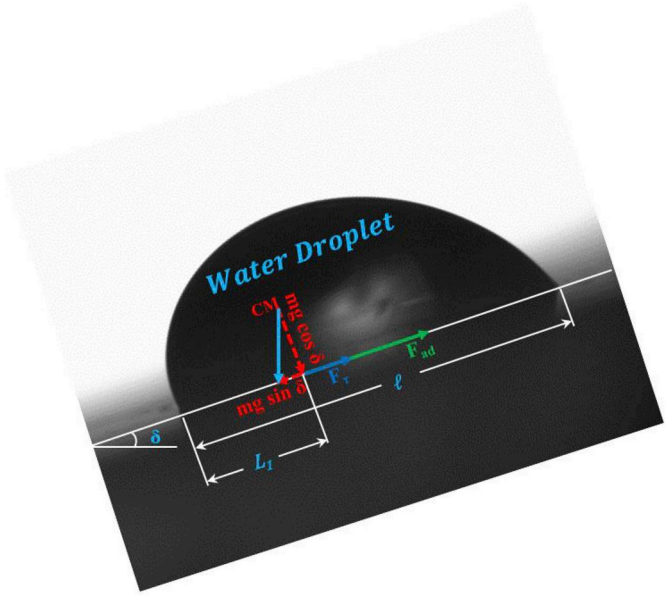

Fig. 4. High speed camera image of a droplet on inclined hydrophilic surface and force diagram.

$$F_L = \frac{24}{\pi^3}\gamma_{LS} d(cos\theta_R - cos\theta_A) \quad (1)$$

where γ_{LS} is the surface tension of the liquid on the solid surface, d is the droplet diameter prior to deformation (same area of the ellipse), θ_R is the receding angle, and θ_A is the advancing angle. Since the solid surface is considered to be smooth, the roughness parameter is not incorporated in equation (1), similar to the Young-Dupre Eq [22].

Under the static condition of the droplet attachment (Fig. 4) at the surface, the net lateral force becomes the same as the lateral force components resulted by the sum of the gravitational force, shear force at the wetted surface, and the adhesion force due to surface tension. In the case of the inclined hydrophilic surface, the droplet undergoes elastic deformation while the net force remains constant. In this case, the line of action of the net force changes inside the droplet volume. As the adhesion force remains higher than the gravitational and shear forces generated on the droplet due to the inclination of the surface, the droplet attaches to the surface. The force balance along the lateral direction at the inclined surface gives rise to:

$$F_{ad} + F_\tau + mgsin\delta \cong \frac{24}{\pi^3}\gamma_{LV} d(cos\theta_R - cos\theta_A) \quad (2)$$

where F_{ad} is the adhesion force, F_τ ($F_\tau = A_w \mu \frac{\partial V}{\partial s}$, A_w is the wetted area, μ is the fluid viscosity, $\partial V/\partial s$ is the rate of fluid strain, and s is direction normal to the inclined surface) is the shear force acting at the wetted surface due to flow developed in the droplet liquid during the inclination, m is the droplet mass, g is the gravity, and δ is the inclination angle of the surface (Fig. 4). Here, the force generated due to the local and convective acceleration of the fluid inside the droplet during the inclination is considered to be negligibly small as compared to the gravitational acceleration of the droplet. Therefore, the force acting on the droplet because of gravity and fluid acceleration is considered to be same as the droplet weight. The re-arrangement of equation (2) yields:

$$F_{ad} \cong \frac{24}{\pi^3}\gamma_{LV} d(cos\theta_R - cos\theta_A) - F_\tau - mgsin\delta \quad (3)$$

Equation (3) is used to obtain the adhesion force acting on the

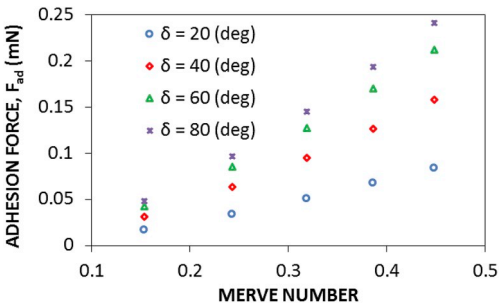

Fig. 5. Adhesion force with Merve number ($= \frac{2\gamma R^2}{3\sigma}$) for various inclination angles of the hydrophobic surface.

droplet at the inclined hydrophilic surface. Since the droplet mass remains the same during the inclination and only changes with droplet volume, a dimensionless force ratio is introduced to account for the droplet volume change. The dimensionless force ratio represents the ratio of the gravitational force over the surface tension force for a given droplet volume, i.e.: $MN = \frac{\gamma R^2}{4\sigma}$, where MN is the Merve number. Fig. 5 shows the adhesion force obtained from equation (3) with MN for various inclination angles. It should be noted that the advancing and the receding angles of the droplet for a given inclination angle are taken from the experimental data, which are given in Table 2. Since contact angle hysteresis increases with both droplet size and the inclination angle of the surface, the adhesion force increases for large droplets at high inclination angles. Although droplet weight lowers adhesion force (equation (3)), the overall increase in adhesion force is associated with increased: i) circumference of the wetted area and ii) droplet hysteresis with large droplet sizes. In addition, increasing inclination angle of the surface enhances the value of $mgsin\delta$ in equation (3); hence, an increase in droplet hysteresis and wetted circumference overcomes the increase of the lateral component of the droplet weight. The shear force, resulting from the flow field generated inside the droplet during droplet inclination, can be determined from the velocity distribution inside the droplet, which is shown in Fig. 6a and b for various inclination angles and two droplet sizes. The shear force generated at the wetted surface due to the flow field inside the droplet changes with droplet size and inclination angles; in which case, it increases with increasing droplet size and inclination angle. The maximum shear force generated is in the order of 8×10^{-7} N, which is significantly less than the adhesion force (0.25×10^{-3} N). Consequently, the influence of shear force on droplet adhesion is negligible, which is true for all the droplet sizes considered in the analysis. The flow field developed inside the droplet forms a single circulation cell for all inclination angles of the surface and droplet sizes (Fig. 6a and b). However, the maximum flow velocity slightly varies inside the droplet; in which case, for a 10 μL droplet and inclination angle $\delta = 20°$, the maximum velocity is in the order of 2.7×10^{-3} m/s while for a 10 μL droplet and inclination angle $\delta = 80°$, it is in the order of 4.52×10^{-3} m/s. Similarly, the maximum velocity for a 20 μL droplet is in the order of 2.7×10^{-3} m/s at inclination angle $\delta = 20°$ and it is

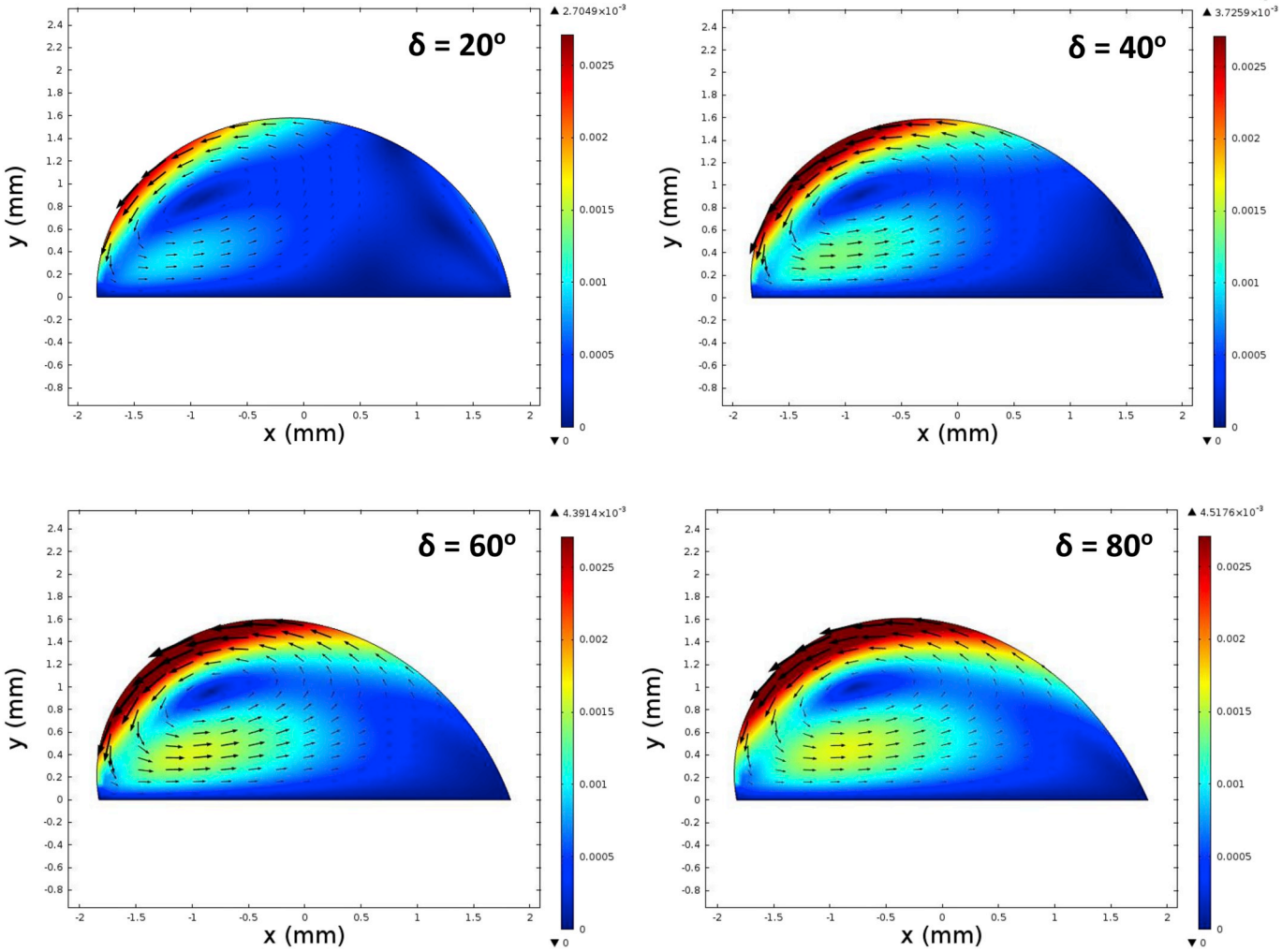

Fig. 6a. Velocity contours inside 10 μL droplet for different inclination angles.

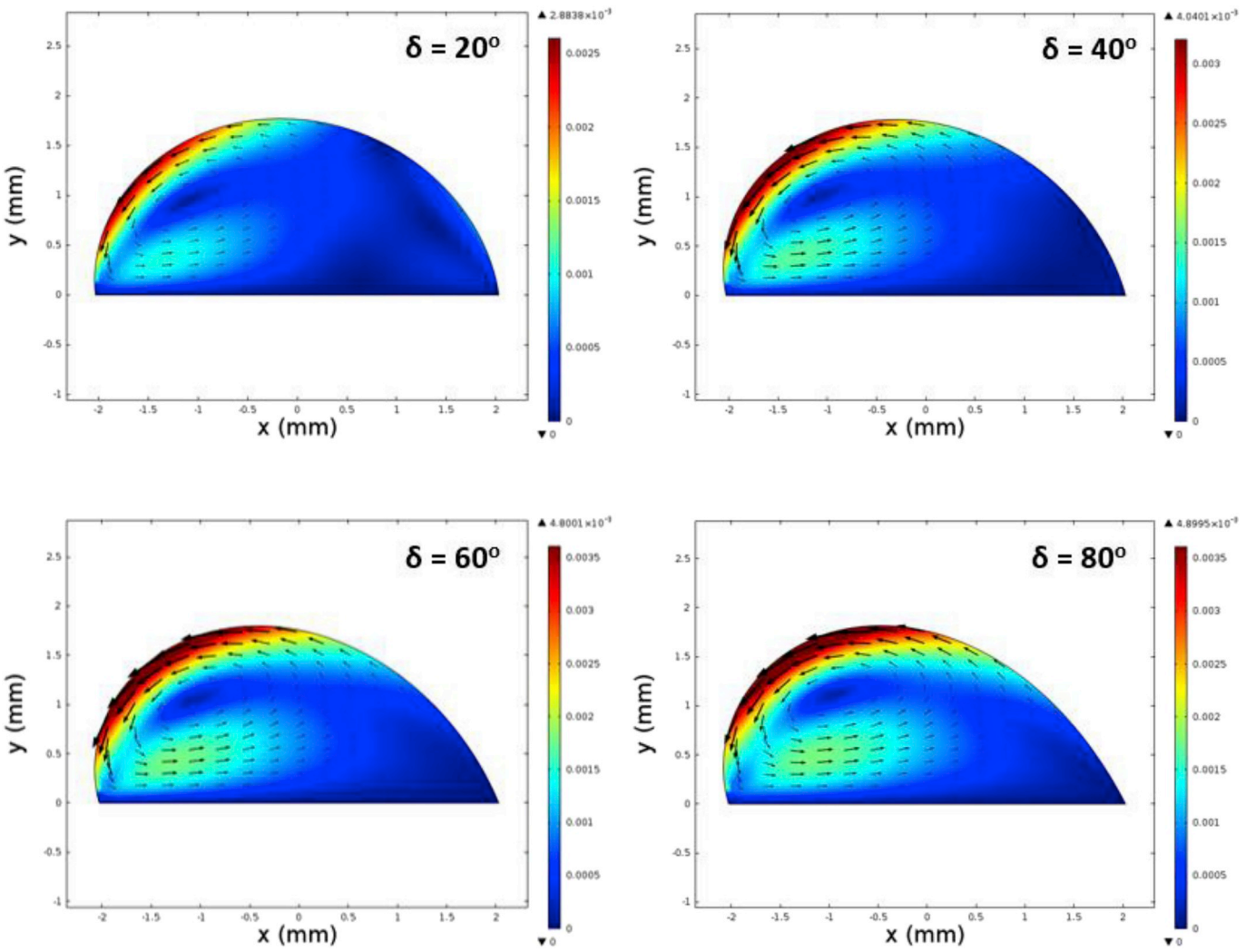

Fig. 6b. Velocity contours inside 20 μL droplet for different inclination angles.

4.65×10^{-3} m/s at inclination angle $\delta = 80°$. Consequently, change of the maximum velocity is notable due to the droplet size; however, the inclination angle has a significant effect on the maximum velocity inside the droplet.

The inclination of the droplet on the hydrophilic surface results in bulging of the droplet for which the droplet lateral (contact) length and height (puddle thickness, Fig. 7) change. Since the droplet geometry changes with the inclination angle, the droplet contact length and the puddle thickness is formulated analytically in terms of the droplet contact angle and the inclination angle, which is given in Appendix 2. The puddle thickness depends on the droplet contact angle on the surface and the contact length of the droplet. Consequently, it changes with the droplet radius and the inclination angle of the surface. On the other hand, the droplet size is critical for bulging and reforming of the droplet shape under the surface inclination; in which case, the capillarity length ($\kappa^{-1} = \sqrt{\frac{\sigma}{\rho g}}$, where κ^{-1} is the capillarity length, σ is the surface tension, ρ is the density, and g is the center of gravity) associated with the droplet becomes critical. A droplet with diameter smaller than the capillarity length remains spherical on the hydrophilic surface. With droplets having a larger diameter than the capillarity length, bulge and large puddle formation occurs. Fig. 8 shows normalized puddle thickness ($\frac{h}{\kappa^{-1}}$, where h is the puddle thickness, κ^{-1} is the capillarity length ($\kappa^{-1} = \sqrt{\frac{\sigma}{\rho g}}$) of the droplet) with Merve number, which is $MN = \frac{\gamma_w a^2}{4\sigma}$, where γ_w is the specific weight of water, a is the droplet diameter and σ is the surface tension of water. Normalized puddle thickness increases with increasing MN. This indicates that increasing droplet size enhances the puddle thickness of the droplet on the hydrophilic surface. Moreover, values of puddle thickness remain less than unity, indicating that the droplet height is less than the capillarity length. This is related to the hydrophilic characteristics of the surface; in which case, the droplet contact angle remains less than 90° for all cases. In addition, the change of puddle thickness with inclination angle of the surface remains small. Although bulging takes place with increasing inclination angle (Fig. 8), the change of puddle thickness remains almost the same for all inclination angles. Fig. 9 shows puddle thicknesses, determined from the analytical expression (Appendix 2) and obtained from the measurements, with inclination angle of the surface for MN = 0.15, which corresponds to a 5 μL droplet volume. The difference between both findings are considerably small for all the surface inclination angles considered. In the case of lateral deformation of the droplet, which is parallel to the inclined surface, the change of droplet length in the lateral direction is considerably large. This can be observed from Fig. 10, in which normalized lateral droplet length ($\frac{w}{l}$, where w is the lateral length of the droplet and l is the droplet wetted contact length) is shown for different surface inclination angles for three values of MN. Inclination of the hydrophobic surface results in bulging of the droplet laterally, which is more pronounced for large values of MN (corresponding to large size droplets). The lateral extension of the droplet becomes significant as the inclination angle of the surface increases. However, a further increase in

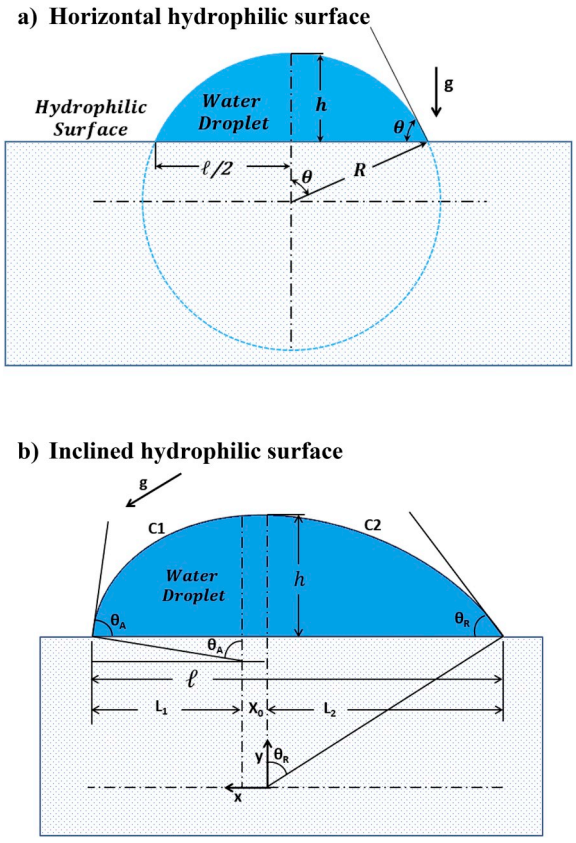

Fig. 7. Droplet geometry used in the analytical formulation for the puddle height (h) and wetted length (l) of the droplet; a) Horizontal hydrophilic surface and b) Inclined hydrophilic surface.

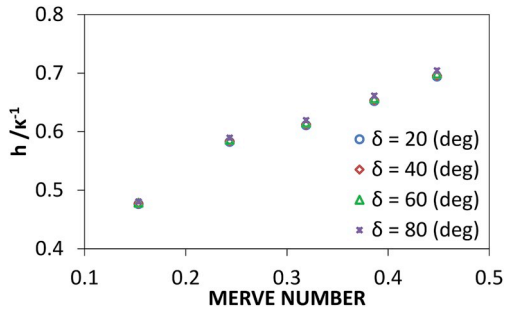

Fig. 8. Normalized puddle thickness ($\frac{h}{\kappa^{-1}}$, where h is the puddle thickness, κ^{-1} is the capillarity length, $\kappa^{-1} = \sqrt{\frac{\sigma}{\rho g}}$) with Merve number ($= \frac{2\gamma R^2}{3\sigma}$) for various inclination angles of hydrophilic surface.

surface inclination angle results in a small change of the lateral extension of the droplet, i.e. the lateral extension of the droplet ceases almost after 60° of inclination angle for MN ≤ 0.24 and 80° for MN ≥ 0.45. The lateral extension of the droplet on the hydrophobic surface modifies the flow field and the maximum velocity inside the droplet (Fig. 6a and b). However, the contact length (wetted length) of the droplet remains the same for individual droplets regardless of the droplet size. Consequently, inclination of the hydrophobic surface does not result in sliding of the droplet for all sizes considered in the analysis. This can be associated with the strong adhesion force generated between the droplet and the inclined hydrophilic surface.

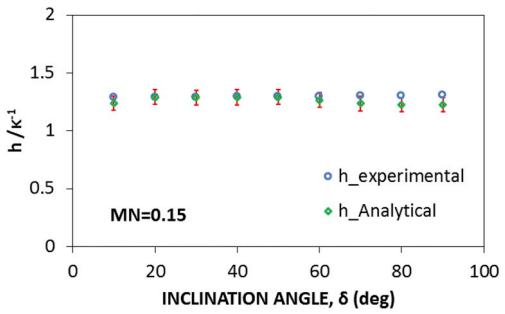

Fig. 9. Normalized puddle thickness obtained from calculations (Eq. (A4)) and experiment for Merve Number = 0.15 (5 μL droplet volume).

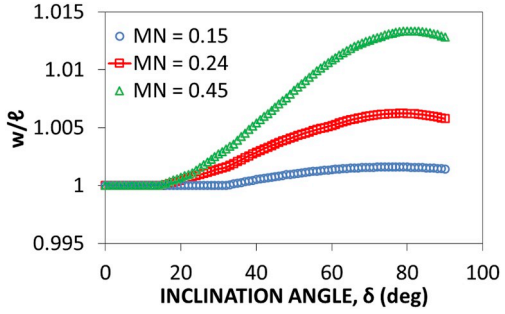

Fig. 10. Normalized lateral extension of droplet ($\frac{w}{l}$, where w is the lateral length of the droplet and l is the wetted length) with inclination angle of hydrophilic surface for various Merve Numbers.

4. Conclusions

Water droplet attachment on a hydrophilic surface with various inclinations is investigated. The geometric features of the droplet due to bulging are formulated and the analytical results are compared with experimental data. The flow field developed inside the droplet is simulated numerically and the predictions validated experimentally using particle image velocimetry (PIV). The findings have revealed that the flow velocity predicted agrees well with the PIV data and the difference between both results is in the order of 6%. The maximum velocity increases with increasing inclination angle and droplet size. The adhesion force increases with increasing Merve number (MN), which is more pronounced at large inclination angles with the hydrophilic surface. Although the inclination of the surface results in an increased lateral component of the gravitational force on the surface, droplet contact angle hysteresis balances out the lateral gravitational force component and increases the adhesion force further. A circulation cell is formed inside the droplet due to the hydrodynamic response of the droplet fluid to the inclination of the surface. The center of rotation and the maximum velocity change with the inclination angle and the size of the droplet. The internal flow generated in the vicinity of the wetted surface contributes to the adhesion force enhancement. The droplet puddle thickness changes slightly with the inclination angle. The lateral extension of the droplet increases with Merve number in a non-linear manner. The present study provides insight into water droplet adhesion on inclined hydrophilic surfaces and provides useful information about the internal fluidity of water droplets.

Acknowledgements

The authors acknowledge the financial support of King Fahd University of Petroleum and Minerals (KFUPM) through Project# IN171001 and King Abdullah City for Atomic and Renewable Energy (K.A.CARE).

Appendix 1. Modelling of internal fluidity of a droplet on inclined hydrophilic surface

In the air and water domains, the incompressible Navier-Stokes equations are solved:

$$\rho\left(\frac{\partial V}{\partial t}+(V-V_M)\cdot\nabla V\right)=-\nabla p+\nabla\left[\mu\left(\nabla V+(\nabla V)^T\right)-\frac{2}{3}\mu(\nabla\cdot V)\right]+F \tag{A1}$$

where V is the fluid velocity, V_M is the mesh velocity, p is the pressure, μ is the dynamic viscosity, and F is the body force per unit volume. In line with the experiments, it is assumed that isothermal condition yields in the solution domain.

The continuity equation yields:

$$\nabla\cdot V=0 \tag{A2}$$

A.1.1 Initial Condition:

Initially water at stagnant condition is considered inside the droplet; in which case, the flow velocity is set to zero and the pressure is set to the Laplace pressure.

A.1.2 Boundary conditions:

The constant pressure boundary is assumed at the droplet outside; in which case, the external pressure of the droplet is set at atmospheric pressure. In addition, stagnant air is considered at the droplet outer surface, which yields zero velocity of the air initially and air drag force is generated during the droplet bulging on the surface. The volume force is applied on the droplet domain in the direction of the inclination angle. To track the evolution of the water-air interface, a fluid-fluid interface is applied to the free boundary of the water droplet:

$$n\cdot(\tau_w-\tau_a)=\sigma(\nabla\cdot n)n-\nabla\sigma \tag{A3}$$

and

$$\tau_{w,a}=-p_{w,a}I+\mu_{w,a}\left(\nabla V_{w,a}+(\nabla V_{w,a})^T\right) \tag{A4}$$

where $\boldsymbol{n}$ is the normal vector, σ is the surface tension and τ is the total stress tensor. Subscripts w and a are for water and air, respectively.

This boundary condition can be decomposed into a normal component:

$$n\cdot\tau_w\cdot n-n\cdot\tau_a\cdot n=\sigma(\nabla\cdot n) \tag{A5}$$

and a tangential component:

$$n\cdot\tau_w\cdot t-n\cdot\tau_a\cdot t=\nabla\sigma\cdot t \tag{A6}$$

The term on the right-hand side of equation (A5) is the force per unit area due to local curvature of the interface. The term on the right-hand side of equation (A6) is a tangential stress associated with the gradients in the surface tension coefficient. A mesh velocity equal to the fluid velocity is imposed on the interface:

$$V_M=V \tag{A7}$$

Free deformation is considered in the fluid flow domain to account for the movement of the water-air interface. Navier Slip boundary condition is considered at the bottom boundary in which it enforces the slip condition ($V.n_{wall}=0$) and takes into account a frictional force, ($F_{fr}=-\frac{\mu}{\beta}V$) where β is the slip length $\left(\beta=\frac{\xi}{2}\right)$ where ξ is the mesh element size. Open boundary conditions are specified to the left and right edges while symmetry boundary condition was considered at the top boundary of the computational domain. Since the time taken for the experiment and the simulation of experimental conditions is short, the evaporation from the droplet surface is neglected in the simulations. This situation is verified during the experiment and the sessile droplet images are taken after 30 s and 100 s periods and it is compared with the image corresponding to that of the start of the experiment. It is noticed that both images have the identical diameter and height of the droplet. In the numerical approach, finer meshes are located in the region near to the water-air interface. Mesh independence tests are conducted for each droplet contact angle considered in the simulations. After the mesh independence tests, as an example, the mesh size comprising of 11712 cells is selected to realize the simulations (for 25 μL droplet). The governing equations of flow are discretized using the backward Euler finite difference method. The implicit scheme with a backward difference approximation is used and unconditionally stable solutions are ensured [23]. The selection of time step is critical to ensure the accuracy of the scheme; in which case, it is in the order of 10^{-4} s. The residuals of flow parameters are set as $\left|\psi^k-\psi^{k-1}\right|\leq 10^{-8}$.

Appendix 2. Formulation of droplet geometric feature

Consider the water droplet on a horizontal hydrophilic surface as shown in Fig. 7a. The following geometric relations can be written for the droplet puddle thickness (h):

$$\sin\theta=\frac{\ell}{2R} \tag{A8}$$

$$\cos\theta = \frac{R-h}{R} \tag{A9}$$

$$R = \frac{\ell}{2\sin\theta} \tag{A10}$$

where θ is the droplet contact angle on the hydrophilic surface, R is the imaginary radius, and l is the droplet contact length and equals to the contact area diameter. The droplet puddle thickness (h) yields:

$$h = R(1-\cos\theta) \tag{A11}$$

Equation (A4) is used to compute the droplet puddle height for various droplet sizes.

In the case of the inclined surfaces, the droplet undergoes an elastic deformation (bulging). The droplet advancing (θ_A) and receding (θ_R) angles are changed during the inclination of the surface as shown in Fig. 7b.

In line with the previous study [24], the following relations can be written:

$$\frac{L_1}{\sin\theta_1} - \frac{L_1}{\sin\theta_1}cos\theta_1 = \frac{L_2}{\sin\theta_2} - \frac{L_2}{\sin\theta_2}cos\theta_2 \tag{A12}$$

Simplifying, L_1 can be expressed as

$$L_1 = L_2 L_f \tag{A13}$$

where

$$L_f = \frac{\sin\theta_1(1-\cos\theta_2)}{\sin\theta_2(1-\cos\theta_1)} \tag{A14}$$

Since $L_1 + L_f = \ell$, the variables L_1 and L_2 can be expressed as

$$L_2 = \frac{\ell \quad L_f}{1+L_f} \tag{A15}$$

and

$$L_1 = \frac{\ell}{1+L_f} \tag{A16}$$

Equations A15 and A16 are used to determine the contact length of the droplet on the inclined surface.

References

[1] Al-Sharafi A, Yilbas BS, Sahin AZ, Ali H, Al-Qahtani H. Heat transfer characteristics and internal fluidity of a sessile droplet on hydrophilic and hydrophobic surfaces. Appl Therm Eng 2016;108:628–40.

[2] Ebert D, Bhushan B. Wear-resistant rose petal-effect surfaces with superhydrophobicity and high droplet adhesion using hydrophobic and hydrophilic nanoparticles. J Colloid Interface Sci 2012;384:182–8.

[3] Bhushan B, Jung YC. Wetting, adhesion and friction of superhydrophobic and hydrophilic leaves and fabricated micro/nanopatterned surfaces. J Phys Condens Matter 2008;20:225010.

[4] Moronuki N, Tachi H, Suzuki Y. Hydrophilic/hydrophobic surface pattern design for oil repellent function in water. Int J Nanomanufacturing 2015;11:46–55.

[5] Yang X, Liu X, Lu Y, Song J, Huang S, Zhou S, Jin Z, Xu W. Controllable water adhesion and anisotropic sliding on patterned superhydrophobic surface for droplet manipulation. J Phys Chem C 2016;120:7233–40.

[6] Shi Y, Tang G, Xia H. Investigation of coalescence-induced droplet jumping on superhydrophobic surfaces and liquid condensate adhesion on slit and plain fins. Int J Heat Mass Transf 2015;88:445–55.

[7] Ou J, Shi Q, Wang Z, Wang F, Xue M, Li W, Yan G. Sessile droplet freezing and ice adhesion on aluminum with different surface wettability and surface temperature. Sci China Phys Mech Astron 2015;58:1–8.

[8] Zhang Z, Yang J, Men X, Xu X, Zhu X. Reversible switching of surface wettability and water adhesion on a polymer nano-composite coating. J Adhes Sci Technol 2012;26:1083–91.

[9] Kwon YH, Myong MH. Numerical analysis for actual droplet movement on hydrophilic/hydrophobic surfaces. In: Hacra 2014 - proceedings of the 7th Asian conference on refrigeration and air conditioning; 2014.

[10] Chang Q, Alexander J. Analysis of single droplet dynamics on striped surface domains using a lattice Boltzmann method. Microfluid Nanofluidics 2006;2:309–26.

[11] Chen H, Dong E, Li J, Stone HA. Adhesion of moving droplets in microchannels. Appl Phys Lett 2013;103:131605.

[12] Liu X, Liu Z, Liang Y, Zhou F. In situ surface reaction induced adhesion force change for mobility control, droplet sorting and bio-detection. Soft Matter 2012;8:10370–7.

[13] Lee D-G, Oh C-K, Yang S-H, Han S-J, Jeong O-C. Fabrication of hydrophilic poly (dimethylsiloxane) with periodic wrinkling surface and its applicationvol. 63. The Transactions of The Korean Institute of Electrical Engineers; 2014. p. 671–5.

[14] Gogolides E, Ellinas K, Tserepi A. Hierarchical micro and nano structured, hydrophilic, superhydrophobic and superoleophobic surfaces incorporated in microfluidics, microarrays and lab on chip microsystems. Microelectron Eng 2015;132:135–55.

[15] Al-Sharafi A, Ali H, Yilbas BS, Sahin AZ, Khaled M, Al-Aqeeli N, Al-Sulaiman F. Influence of thermalcapillary and buoyant forces on flow characteristics in a droplet on hydrophobic surface. Int J Therm Sci 2016;102:239–53.

[16] Al-Sharafi A, Yilbas BS, Ali H, Sahin AZ. Internal fluidity of a sessile droplet with the presence of particles on a hydrophobic surface. Numer Heat Transf, Part A: Applications 2016;70:1118–40.

[17] http://www.comsol.com/comsol-multiphysics; 2017.

[18] Erzincanli B, Sahin M. An arbitrary Lagrangian–Eulerian formulation for solving moving boundary problems with large displacements and rotations. J Comput Phys 2013;255:660–79.

[19] Al-Sharafi A, Sahin AZ, Yilbas BS. Measurement of thermal and electrical properties of multiwalled carbon nanotubes–water nanofluid. J Heat Transf 2016;138:072401.

[20] ElSherbini A, Jacobi A. Retention forces and contact angles for critical liquid drops on non-horizontal surfaces. J Colloid Interface Sci 2006;299:841–9.

[21] Pilat D, Papadopoulos P, Schaffel D, Vollmer D, Berger R, Butt H-J. Dynamic measurement of the force required to move a liquid drop on a solid surface. Langmuir 2012;28:16812–20.

[22] Ayyad AH. Thermodynamic derivation of the Young–Dupré form equations for the case of two immiscible liquid drops resting on a solid substrate. J Colloid Interface Sci 2010;346:483–5.

[23] He Q, Jiao D. Explicit and unconditionally stable time-domain finite-element method with a more than "optimal" speedup. Electromagnetics 2014;34:199–209.

[24] ElSherbini A, Jacobi A. Liquid drops on vertical and inclined surfaces: I. An experimental study of drop geometry. J Colloid Interface Sci 2004;273:556–65.